Near Infrared Luminescent Oxygen Nanosensors with Nanoparticle Matrix Tailored Sensitivity

Yong-Eun Koo Lee,[†] Elyse E. Ulbrich,[†] Gwangseong Kim,[†] Hoejin Hah,[†] Christen Strollo,[†] Wenzhe Fan,[†] Rajan Gurjar,[‡] SangMan Koo,[§] and Raoul Kopelman*,[†]

Department of Chemistry, University of Michigan, Ann Arbor, Michigan, Advanced Sensor Development Group, Radiation Monitoring Devices, Inc., Watertown, Massachusetts, and Department of Chemical Engineering, Hanyang University, Seoul, Korea

The development of sensors for noninvasive determination of oxygen levels in live cells and tissues is critical for the understanding of cellular functions, as well as for monitoring the status of disease, such as cancer, and for predicting the efficacy of therapy. We describe such nontoxic, targeted, and ratiometric 30 nm oxygen nanosensors made of polyacrylamide hydrogel, near-infrared (NIR) luminescent dyes, and surface-conjugated tumor-specific peptides. They enabled noninvasive real-time monitoring of oxygen levels in live cancer cells under normal and hypoxic conditions. The required sensitivity, brightness, selectivity, and stability were achieved by tailoring the interaction between the nanomatrix and indicator dyes. The developed nanosensors may become useful for in vivo oxygen measurements.

Oxygen is one of the key metabolites in aerobic systems and plays important biological roles. Maintaining oxygen homeostasis is critical for cellular function, proliferation, and survival, and an oxygen concentration below or above the demanded level for each cellular organ can be a possible cause of disease as well as an indicator for disease. Hypoxia, i.e., poor oxygenation, is especially an important factor in tumor biology and in cancer treatment. It is a common characteristic of locally advanced solid tumors and has been revealed to promote angiogenesis, tumor aggressiveness, local recurrence, and metastasis.[1-3] Hypoxia is also known to cause resistance to various therapies, including photodynamic therapy, radiotherapy, and chemotherapy.[3,4] Therefore, the development of a noninvasive tool that directly and repeatedly measures the distribution heterogeneity of the partial oxygen pressure inside a growing tumor would be of considerable use in the clinic.

The standard tool for measuring hypoxia has been a 250−350 μm polarographic electrode. Its drawbacks are that it is physically quite invasive[4-6] and that it consumes a finite amount of oxygen during each measurement, resulting in an underestimation of the oxygen levels when used for continuous monitoring. Luminescent fiber optical oxygen sensors have also been introduced in animal models for such oxygen monitoring.[7,8] The oxygen sensing mechanism is based on the oxygen-dependent luminescence quenching of an oxygen sensitive dye. Singlet oxygen, a quenching reaction side-product, can react with the surrounding molecules, and therefore, oxygen can be consumed. However, the oxygen consumption by the luminescence sensor is usually often negligible with short illumination times, as singlet oxygen has a very short lifetime in the aqueous phase and it is produced only during illumination of light. The fiber sensor, however, is still an invasive tool due to its size (250−630 μm). In vivo measurements of oxygen have been performed recently by various imaging techniques, such as positron emission tomography (PET),[9,10] magnetic resonance imaging (MRI),[11,12] and luminescence imaging,[13-18] usually after injecting suitable molecular probes. While the methods using molecular probes may enable noninva-

* Corresponding author. E-mail: kopelman@umich.edu.
† University of Michigan.
‡ Radiation Monitoring Devices, Inc.
§ Hanyang University.

(1) Young, S. D.; Marshall, R. S.; Hill, R. P. *Proc. Nat. Acad. Sci. U.S.A.* **1988**, *85*, 9533–9537.
(2) Semenza, G. L. *J. Clin. Invest.* **2001**, *108*, 39–40.
(3) Arbeit, J. M.; Brown, J. M.; Chao, K. S. C.; Chapman, J. D.; Eckelman, W. C.; Fyles, A. W.; Giaccia, A. J.; Hill, R. P.; Koch, C. J.; Krishna, M. C.; Krohn, K. A.; Lewis, J. S.; Mason, R. P.; Melillo, G.; Padhani, A. R.; Powis, G.; Rajendran, J. G.; Reba, R.; Robinson, S. P.; Semenza, G. L.; Swartz, H. M.; Vaupel, P.; Yang, D. *Int. J. Radiat. Biol.* **2006**, *82*, 699–757.
(4) Nordsmark, M.; Bentzen, S. M.; Rudat, V.; Brizel, D.; Lartigau, E.; Stadler, P.; Becker, A.; Adam, M.; Molls, M.; Dunst, J.; Terris, D. J.; Overgaard, J. *Radiother. Oncol.* **2005**, *77*, 18–24.

(5) Schiff, S. J.; Somjen, G. G. *Brain Res.* **1985**, *344*, 150–153.
(6) Vaupel, P.; Hockel, M.; Mayer, A. *Antioxid. Redox Signaling* **2007**, *9*, 1221–1235.
(7) Seddon, B. M.; Honess, D. J.; Vojnovic, B.; Tozer, G. M.; Workman, P. *Radiat. Res.* **2001**, *155*, 837–846.
(8) Brurberg, K. G.; Graff, B. A.; Rofstad, E. K. *Br. J. Cancer* **2003**, *89*, 350–356.
(9) Zanzonico, P.; O'Donoghue, J.; Chapman, J. D.; Schneider, R.; Cai, S.; Larson, S.; Wen, B.; Chen, Y.; Ronald Finn, R.; Ruan, S.; Gerweck, L.; Humm, J.; Ling, C. *Eur. J. Nucl. Med. Mol. Imaging* **2004**, *31*, 117–128.
(10) Lewis, J. S.; Herrero, P.; Sharp, T. L.; Engelbach, J. A.; Fujibayashi, Y.; Laforest, R.; Kovacs, A.; Gropler, R. J.; Welch, M. J. *J. Nucl. Med.* **2002**, *43*, 1557–1569.
(11) Zhao, D.; Ran, S.; Constantinescu, A.; Hahn, E. W.; Mason, R. P. *Neoplasia* **2003**, *5*, 308–318.
(12) Kodibagkar, V. D.; Wang, X.; Pacheco-Torres, J.; Gulaka, P.; Mason, R. P. *NMR Biomed.* **2008**, *21*, 899–907.
(13) Dunphy, I.; Vinogradov, S. A.; Wilson, D. F. *Anal. Biochem.* **2002**, *310*, 191–198.
(14) Ziemer, L. S.; Lee, W. M. F.; Vinogradov, S. A.; Sehgal, C.; Wilson, D. F. *J. Appl. Physiol.* **2005**, *98*, 1503–1510.
(15) Wilson, D. F.; Lee, W. M. F.; Makonnen, S.; Finikova, O.; Apreleva, S.; Vinogradov, S. A. *J. Appl. Physiol.* **2006**, *101*, 1648–1656.
(16) Lebedev, A. Y.; Cheprakov, A. V.; Sakadzic, S.; Boas, D. A.; Wilson, D. F.; Vinogradov, S. A. *ACS Appl. Mater. Interfaces* **2009**, *1*, 1292–1304.
(17) Yaseen, M. A.; Srinivasan, V. J.; Sakadzic, S.; Wu, W.; Ruvinskaya, S.; Vinogradov, S. A.; Boas, D. A. *Opt. Express* **2009**, *17*, 22341–22350.
(18) Zhang, S.; Hosaka, M.; Yoshihara, T.; Negishi, K.; Iida, Y.; Tobita, S.; Takeuchi, T. *Cancer Res.* **2010**, *70*, 4490–4498.

sive detection of oxygen in vivo, they are subject to the following problems from molecular probes: (1) being sequestered unevenly into various cell compartments; (2) nonspecific protein binding that affects the measurements; (3) the available molecular probes may be cytotoxic or have to be modified into a cell-permeable form. Furthermore, molecular probes typically have a short plasma lifetime and no selectivity toward specific targets, and thus, only a small fraction of the molecular probes reaches the specific location of interest within the body.

Recently, macromolecular probes conjugated with polyethylene glycol (PEG) have been reported to avoid some of the above problems with molecular probes.[15,16] However, these problems may be avoided relatively easily by replacing the molecular probes with nanoparticle-based probes because of many potential advantages from their size and engineerability.[19-22] The use of nanoparticles is especially advantageous for in vivo cancer applications. Nanoparticles can efficiently deliver therapeutic/imaging/sensing agents to tumors by the so-called "enhanced permeability and retention" (EPR) effect[23] and facile surface modifications with suitable targeting moieties and PEG chains. Fluorescent nanoparticle-based sensors, often called PEBBLE (photonic explorers for biomedical use with biologically localized embedding) nanosensors, have been successfully developed for measuring oxygen concentrations inside or in the proximity of live cells.[24-28] These nanosensors were made of oxygen-sensitive dyes embedded within a nanoparticle matrix, and the oxygen sensing mechanism is the same as the luminescent fiber sensor. Note that the luminescent oxygen nanosensors have higher signals at lower oxygen levels, which is advantageous for measurements in the low oxygen, hypoxic tumor tissue. Such nanosensors, however, have not yet been applied for in vivo oxygen sensing. This may be partly because of the poor aqueous solubility of the previously reported oxygen nanosensors,[24-29] which were mostly made of hydrophobic oxygen molecular probes and hydrophobic matrixes so as to have high loading of probes and high oxygen solubility and permeability.[30-33] It may also have been due to the low tissue penetration depth for photons at the specific excitation and/or emission wavelength (in the visible range) of those indicator dyes, as well as a lack of sufficient sensitivity. In addition, previous nanosensors were not surface-modified for specific biological targeting.

In this study, we developed ratiometric luminescent nanoparticle-based sensors by incorporating the oxygen-sensitive Pd-tetra-(4-carboxyphenyl) tetrabenzoporphyrin dendrimer (G2),[13-15,34-36] as well as an oxygen-insensitive reference dye (Alexa 647 dextran 10 000 or HiLyte 680 SE) into polyacrylamide (PAA) hydrogel nanoparticles. G2 has been applied for in vivo oxygen imaging[13-15] due to its spectral characteristics, an absorption maximum at 630 nm and a NIR emission maximum at 800 nm, which are ideal for deep tissue penetration[37] and free from cellular autofluorescence. The surface of the sensors was modified with peptides that were either universal membrane penetrating peptides (TAT) or tumor-specific peptides for target-specific delivery (F3). The developed nanosensors were successfully applied for intracellular measurements. We believe that these nanosensors are also useful for in vivo applications. Note that the PAA nanoparticles have a high aqueous solubility, a long plasma circulation lifetime (~24 h),[21] and a diameter of about 30 nm, which made them suitable as medical nanodevices for efficient imaging and photodynamic therapy of tumor in rats.[38] Nanoparticles of 10−100 nm in diameter are considered to offer optimal tumor accumulation as they avoid fast renal elimination and recognition by the immune system (e.g., phagocytes) when applied in vivo.[21]

EXPERIMENTAL SECTION

Chemicals and Materials. Acrylamide, methylene-bis-acrylamide (MBA), dioctyl sulfouccinate (AOT), Brij 30, hexane, ammonium persulfate, N,N,N',N'-tetramethyl ethylenediamine (TEMED), N-(3-dimethylaminopropyl)-N'-ethylcarbodiimide hydrochloride (EDC), bovine serum albumin (BSA; 30% w/v), L-cysteine, and 3-(4,5-dimethylthiazolyl-2)-2,5-diphenyltetrazolium bromide (MTT) were all acquired from Sigma-Aldrich (St. Louis, MO). 3-(Aminopropyl)methacrylamide hydrochloride salt (APMA) was obtained from Polysciences Inc. (Warrington, PA). Ethanol (95%) was acquired from Decon laboratories, Inc. (King of Prussia, PA). N-Hydroxysulfosuccinimide (sulfo-NHS) and succinimidyl 4-[N-maleimidomethyl]cyclohexane-1-carboxylate (SMCC) were acquired from Pierce Biotechnology (Rockford, IL). G2 was obtained from Oxygen Enterprises Ltd. (Philadelphia, PA). HiLyte Fluor 680 acid SE was acquired from AnaSpec (San Jose, CA) and Alexa Fluor 647 dextran 10 000 was purchased from Invitrogen (Carlsbad, CA). TAT-Cys peptide (YGRKKRRQRRRC) and F3-Cys peptide (PKAARALPSQRSRPPEKAKKPPDKPAPEKKKC) were purchased from SynBioSci (Livermore, CA). All solutions were prepared in 18 MΩ water purified in a Barnstead 1 Thermolyne Nanopure II system. All the gases, O_2 (extra dry

(19) Koo Lee, Y.; Smith, R.; Kopelman, R. Annu. Rev. Anal. Chem. 2009, 2, 57–76.
(20) Koo Lee, Y.; Kopelman, R. WIREs Nanomed. Nanobiotechnol. 2009, 1, 98–110.
(21) Koo, Y. L.; Reddy, G. R.; Bhojani, M.; Schneider, R.; Philbert, M. A.; Rehemtulla, A.; Ross, B. D.; Kopelman, R. Adv. Drug Delivery Rev. 2006, 58, 1556–1577.
(22) Koo Lee, Y.; Kopelman, R. In Biomedical Nanotechnology, Methods in Molecular Biology Series; Walker, J. M., Ed.; Humana Press: Totowa, NJ (in press, 2010).
(23) Maeda, H. Adv. Enzyme Regul. 2001, 41, 189–207.
(24) Xu, H.; Aylott, J. W.; Kopelman, R.; Miller, T. J.; Philbert, M. A. Anal. Chem. 2001, 73, 4124–4133.
(25) Koo, Y. L.; Cao, Y.; Kopelman, R.; Koo, S. M.; Brasuel, M.; Philbert, M. A. Anal. Chem. 2004, 76, 2498–2505.
(26) Schmalzlin, E.; van Dongen, J. T.; Klimant, I.; Marmodee, B.; Steup, M.; Fisahn, J.; Geigenberger, P.; Lohmannsroben, H. G. Biophys. J. 2005, 89, 1339–1345.
(27) Kuang, Y. N.; Walt, D. R. Biotechnol. Bioeng. 2007, 96, 318–325.
(28) Borisov, S. M.; Klimant, I. Microchim. Acta 2009, 164, 7–15.
(29) Cao, Y.; Koo, Y. L.; Kopelman, R. Analyst 2004, 129, 745–50.
(30) Amao, Y. Microchim. Acta 2003, 143, 1–12.
(31) O'Riordan, T. C.; Zhdanov, A. V.; Ponomarev, G. V.; Papkovsky, D. B. Anal. Chem. 2007, 79, 9414–9419.
(32) Fercher, A.; Ponomarev, G. V.; Yashunski, D.; Papkovsky, D. B. Anal. Bioanal. Chem. 2010, 396, 1793–1803.
(33) Wang, X.; Chen, H.; Zhao, Y.; Chen, X.; Wang, X. Trends Anal. Chem. 2010, 29, 319–338.

(34) Rozhkov, V.; Wilson, D.; Vinogradov, S. Macromolecules 2002, 35, 1991–1993.
(35) Rietveld, I. B.; Kim, E.; Vinogradov, S. A. Tetrahedron 2003, 59, 3821–3831.
(36) Finikova, O. S.; Cheprakov, A. V.; Beletskaya, I. P.; Carroll, P. J.; Vinogradov, S. A. J. Org. Chem. 2004, 69, 522–535.
(37) Vogel, A.; Venugopalan, V. Chem. Rev. 2003, 103, 577–644.
(38) Reddy, G. R.; Bhojani, M. S.; McConville, P.; Moody, J.; Moffat, B. A.; Hall, D. E.; Kim, G.; Koo, Y.; Woolliscroft, M. J.; Sugai, J. V.; Johnson, T. D.; Philbert, M. A.; Kopelman, R.; Rehemtulla, A.; Ross, B. D. Clin. Cancer Res. 2006, 12, 6677–6686.
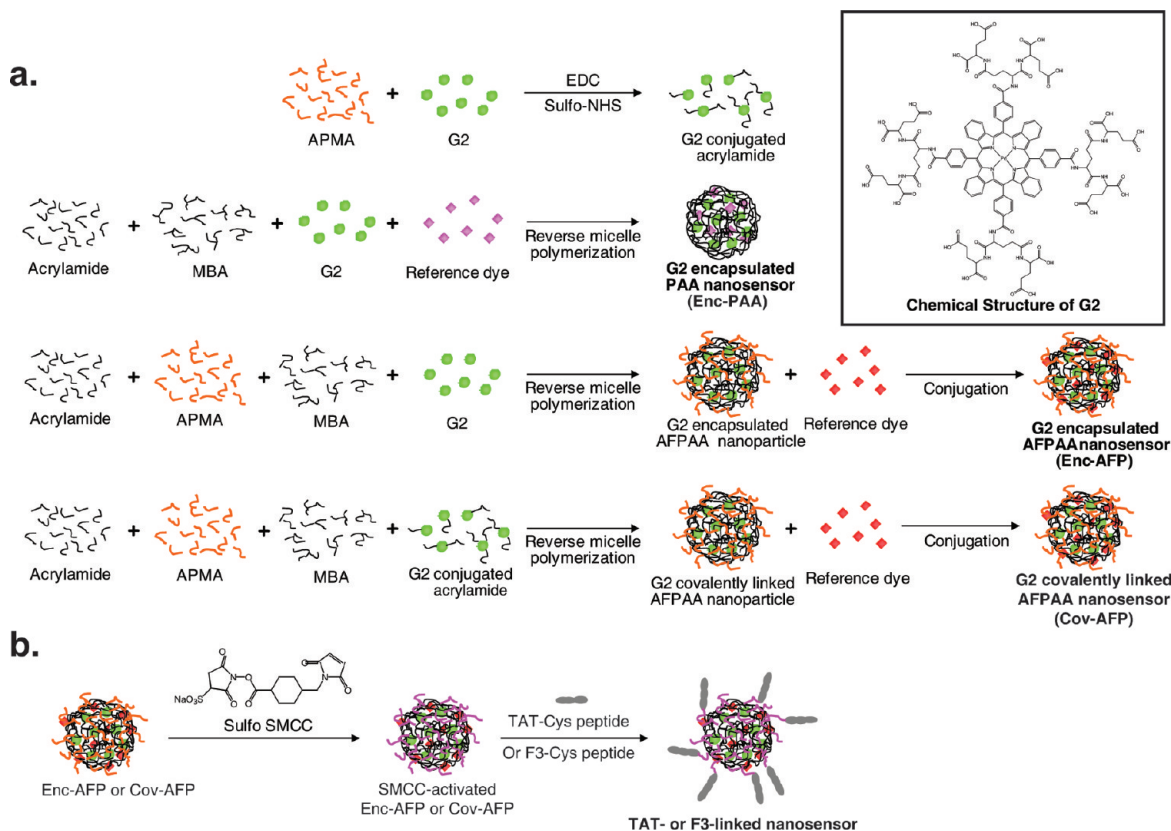
Figure 1. Synthesis of targeted ratiometric G2-loaded oxygen nanosensor. (a) Preparation of three kinds of G2-loaded PAA nanosensors. The input amount of G2, ratio of G2 to APMA, and ratio of EDC to G2 were varied for optimal loading of G2 as in Table 1. (b) Conjugation of TAT or F3 peptide to the G2-loaded AFPAA nanosensor. The targeted G2-loaded ratiometric oxygen sensors were prepared with optimized oxygen sensitivity and brightness.

grade), air (dry grade), N_2 (prepurified), NO (CP grade), and argon, were obtained from Metro Welding Supply (Detroit, MI). All the chemicals and materials were used as received.

Cells. A549 human lung adenocarcinoma cells and C6 glioma cells were used for intracellular oxygen measurements, and MDA-MB-435 and MCF-7 cells were used for tumor targeting tests. The cells were cultured in Dulbecco's modified eagle medium (DMEM) supplemented with 10% fetal bovine serum, 1 mM sodium pyruvate, 100 units/mL penicillin, 100 μg/mL streptomycin sulfate, and 292 μg/mL L-glutamine. All chemicals for cell culture were purchased from Invitrogen.

Preparation of G2-Loaded Nanosensors. The nanosensors were prepared by polymerization of a microemulsion that is formed from a monomer mixture, in an aqueous solution, in hexane with surfactants. The G2 dye was loaded into nanoparticles in three different ways (Figure 1a). For G2-encapsulated nanoparticles, G2 dye was mixed with monomer solution in pH 7.4 phosphate buffer solution (PBS; 1.6 mL) and then added to the argon-purged hexane solution (36 mL) containing Brij 30 (6.85 mmol) and AOT (2.88 mmol) to form a microemulsion. The monomer solution for the PAA nanoparticles contains acrylamide (8.6 mmol) and MBA (1.2 mmol) and that for the amine-functionalized PAA (AFPAA) nanoparticles contains APMA (0.25 mmol) in addition to the acrylamide and MBA. Nanoparticle synthesis was initiated by ammoninum persulfate (2.8×10^{-5} mmol) and TEMED (0.54 mmol). The solution was stirred overnight under argon at room temperature. The hexanes were then evaporated using a Rotavapor-R (Brinkmann Instruments).

The resultant thick residue was transferred to an Amicon ultrafiltration cell (Millipore Corp., Bedford, MA), washed thoroughly with ethanol and water, and then freeze-dried with a 5 L ModulyoD freeze-dryer (ThermoFisher Scientific). For G2 covalently linked AFPAA nanoparticles, G2 dye was first mixed with EDC and sulfo-NHS for 15 min and then mixed with the same monomer solution as that for G2 encapsulated AFPAA nanoparticles at 37 °C for 2 h. The molar amount of sulfo-NHS was 2.5 times that of EDC. The mixture solution was then polymerized as described for the preparation of G2 encapsulated nanoparticles. For G2 covalently linked AFPAA nanoparticles with encapsulated BSA, the procedure is the same except that BSA (2.5 mg) was added to the G2–monomer mixture solution. Reference dyes that can be excited at the same wavelength as G2 (630 nm), as well as fluoresce at a wavelength between the two G2 peaks (645 and 804 nm), were coloaded into the nanoparticles, so as to make ratiometric nanosensors (Figure 1a). For the PAA nanoparticles, Alexa 647 dextran 10 000 was mixed with the monomer solution and G2 dye and encapsulated during polymerization. For the AFPAA nanoparticles, HiLyte 680 SE was mixed with the G2 encapsulated or covalently linked AFPAA nanoparticles in pH 7.4 PBS and stirred for 2 h, and then, the nanoparticle solution was thoroughly washed with water. Note that Alexa 700 SE was initially tried but replaced with Hilyte 680 SE because of the pH sensitivity of Alexa 700 SE after being conjugated to nanoparticles, showing a 30−40% difference in the fluorescence intensity between pH 5 and 9.

Table 1. Dye Loading Efficiency and Oxygen Sensitivity of Various G2-Loaded Nanosensors

nanosensor ID[a]	input G2/total monomer (μg/mg)	EDC/G2 (mol/mol)	APMA/G2 (mol/mol)	dye-loading efficiency[b] (%)	dye loading per nanosensors (% wt)	sensitivity[c] R_{N2}/R_{Air}	R_{N2}/R_{O2}	$Q_{DO\text{-}Air}$ (%)	$Q_{DO\text{-}O2}$ (%)
Enc-PAA	2.6			0.7	0.0018	6.8	23	85	96
Enc-AFP-1	2.9		540	24	0.069	3.7	9.9	73	90
Enc-AFP-2	4.5		188	22	0.099	5.4	17	82	94
Cov-AFP-1	2.5	92	676	62	0.16	2.3	6.6	57	85
Cov-AFP-2	4.5	98	419	67	0.30	4.7	13	79	92
Cov-AFP-3	4.7	18	188	64	0.30	8.0	28	88	96
Cov-AFP-4	9.5	8.9	93	46	0.44	7.4	25	87	96
Cov-AFP-5	16.8	18	53	72	1.2	7.5	25	87	96
Cov-AFP with BSA	4.8	18	188	21	0.10	2.9	6.6	66	85

[a] The nanosensor ID indicates the dye loading method as well as the nanoparticle matrix. Enc and Cov denote encapsulation and covalent bonding of G2 dyes inside nanoparticles, respectively, while PAA and AFP denote polyacrylamide and amine-functionalized polyacrylamide matrixes, respectively. [b] The dye loading efficiency is defined as the percentage of the loaded dye amount with respect to the input amount. [c] The sensitivity values in this table, represented by $R_{N2}/R_{Air \, (or \, O2)}$ and Q_{DO}, were measured at room temperature.

Preparation of TAT or F3 Peptide Conjugated Nanosensors. TAT or F3 peptides were conjugated to the surface of the nanosensors, for universal or specific targeting, respectively (Figure 1b). The detailed procedure is as follows: The freeze-dried G2-loaded AFPAA nanosensors (50 mg) were dissolved in pH 7.2 PBS (2.5 mL), treated with SMCC (2 μmol), and stirred at room temperature for 30 min. The reaction mixture was then subjected to thorough washings to remove any unreacted ligands and concentrated to ~20 mg/mL. TAT-Cys (0.02 μmol) or F3-Cys peptides (0.06 μmol) were added to the concentrated nanosensor solution and gently stirred overnight (>8 h) at room temperature and treated with L-cysteine (1 μmol) for another 2 h. The resultant solution was thoroughly washed with water and PBS in an Amicon cell. For the tumor cell targeting experiment, nontargeted oxygen nanosensors were also prepared by capping the surface amine groups with L-cysteine using the same conjugation procedure in order to minimize nonspecific interactions with anionic cell surface membranes or cellular uptake.

Size Characterization. The size of the nanosensors in dried powder form was measured by scanning electron microscopy (SEM) using a Phillips XL30 scanning electron microscope. The size distribution of the nanosensors in an aqueous solution was measured by dynamic light scattering (DLS) using a Beckman-Coulter DelsaNano C Zeta potential/submicrometer size analyzer.

Dye Loading Efficiency. A calibration curve of the absorbance of G2 vs the dye concentration was constructed after measuring the absorbance of a series of the free G2 dye aqueous solutions of known concentrations using a Shimadzu UV-1601 spectrometer. The loaded amount of G2 per nanoparticle was then determined by comparing the absorbance of a nanosensor aqueous suspension with the calibration curve. The dye loading efficiency was determined by calculating the percentage of the loaded amount of G2 dye per nanoparticle with respect to the input amount of G2 per total amount of monomer used during synthesis.

Dye Leaching. A nanosensor suspension of 10 mg/mL in PBS or PBS containing 9% (w/w) BSA was prepared in an Amicon ultrafiltration cell and stirred for an hour, and the filtrate was collected. The luminescence of the filtrate was measured by a FluoroMax-3 spectrofluorometer (HORIBA Jobin Yvon). The nanosensors were reconstituted in PBS to make 10 mg/mL, and the same procedure was repeated over the observation period (1 or 3 days).

Peptide Amount per Nanosensors. The conjugated amount of peptides was determined by quantitative amino acid analysis (QAAA).

Sensitivity, Reversibility, and Calibration. An aqueous nanosensor suspension was prepared and placed in a gastight glass cell. The solution at specified temperature was then purged for 30 min at a 70 mL/min flow rate with air, O_2, N_2, and their mixtures with varying ratios through a gas mixer (Cole Parlmer Instrument Co), respectively. The luminescence spectra of each purged solution were taken, and the intensity ratio of G2/reference dye (R) was calculated from each spectrum. For sensitivity measurements, R_{N2}/R_{Air}, R_{N2}/R_{O2}, $Q_{DO\text{-}Air}$, and $Q_{DO\text{-}O2}$ were calculated. Q_{DO} (DO denotes dissolved oxygen) represents the overall quenching response between a nitrogen-saturated and air-saturated or oxygen-saturated condition, which is defined as, $Q_{DO\text{-}Air \, (or \, O2)} = (R_{N2} - R_{Air \, (or \, O2)})/R_{N2} \times 100$.

For calibration, the ratio of R_0 (R at oxygen free condition or R_{N2}) to R was calculated, and the oxygen concentration of each gas-purged solution was measured using an oxygen electrode (Fisher Scientific, Inc.). A calibration curve based on the linear Stern–Volmer equation ($R_0/R = K_{SV}^{conc}[O_2] + 1$, where K_{SV}^{conc} is the Stern–Volmer constant and $[O_2]$ is the dissolved oxygen concentration) was then constructed. Note that the luminescence spectra of the nanosensors were taken by a fluorescence microscope rather than by the spectrofluorometer, so as to reduce scattering interference from the presence of nanoparticles. An Olympus IMT-II inverted fluorescence microscope was used, which is equipped with an Acton Research Corp. spectrograph, a Hamamatsu HC230 CCD, and a Xenon lamp (Sutter Instrument, Novato, CA) with an Omega filter cube (Excitation filter 610DF70, dichroic mirror 660 DRLP and long-pass emission filter 674ALP).

Photostability. A nanosensor suspension in PBS (typically 5 mg/mL) or a free dye solution of the same G2 concentration as in the nanosensor solution was submitted to continuous illumination of a 630 nm light for 1 h. The luminescence intensity was taken every 1 min.

Interference from BSA, pH, and NO. Nanosensor suspensions of 2 mg/mL in PBS or free dye solutions of the same G2 concentration as in the nanosensor solution, with and without interfering chemicals, were prepared, and their luminescence

spectra were taken. The BSA concentration varied from 0 to 9.3% (w/w), and the pH varied from 3 to 10. The NO concentration was fixed at about 150 ppb, and the test solution was prepared as follows: A 2 mL aliquot of nanosensor suspension or free dye solution was prepared in a gastight container and purged with argon for 20 min. A 5 μL aliquot of NO saturated stock solution, prepared according to a previously described method,[39] having the estimated concentration of ~61 ppm at 22 °C,[40] was then added to each prepared solution.

Nanosensor Delivery into Cells and Oxygen Measurements. For intracellular oxygen measurements, oxygen nanosensors were delivered into cells through endocytosis, TAT peptide, or gene gun. For endocytosis or TAT-assisted delivery, the cells were treated with the nanosensors in the following way: incubation with plain or TAT-linked nanosensors of 2−4 mg/mL in cell medium at 37 °C and subsequently washed three times with cell culture medium without phenol red indicator. The cells with fresh cell medium were then placed on the inverted fluorescent microscope for imaging or taking spectra. The typical incubation time was overnight (>8 h) for plain nanosensors and 1−4 h for TAT-linked nanosensors. For gene-gun delivery, a thin film of the nanosensors suspended in water was dried on the target membrane and delivered into cells located at 45 mm below the membrane at a firing pressure of 900−1000 psi using a BioRad (Hercules, CA) Biolistic PDS-1000/He Gene Gun system. After gene-gun delivery, the cells with fresh cell medium were placed in a nonsterile incubator for 30 min before experimentation. Luminescence images of nanosensor-loaded cells were obtained, using 633 nm excitation and a bandpass filter transparent between 650 and 750 nm, on an Olympus FluoView 500 confocal laser scanning microscope equipped with Olympus FV-500 software and a HeNe laser. Luminescence spectra of the nanosensors were taken as described above in the sensitivity measurements. The concentrations of D-glucose and glucose oxidase used to induce the change in extracellular oxygen concentration were 10 mM and 10 units per mL, respectively. The extracellular oxygen concentration measurements were taken immediately after adding the nanosensors over the cells, to minimize the cellular uptake.

Target-Specific Delivery by F3-Linked Nanosensors. Two different cell lines (MDA-MB-435, MCF-7) were incubated with 2 mg/mL of F3-linked and nontargeted oxygen nanosensors for 30 min at 37 °C and washed three times with cell medium. Confocal images were obtained with 633 nm excitation and 660 nm long-path emission filters, on an Olympus Fluoview 300 confocal system connected with Olympus IX70 microscope. The cell targeting efficiency of the F3 peptide was quantified by analyzing pixel intensity per cells on confocal images.

MTT Assay. Cells were cultivated on 96-well plates. For each treatment with nanoparticles and for a control (cells without any treatment), 12 wells were used for reliable measurements. The oxygen nanosensors were added to a cell medium to make the nanoparticle sensor concentration to be 1, 2, and 4 mg/mL. For comparison, blank PAA nanoparticles were also added to a cell medium at the concentration of 4 mg/mL. After 1, 4, or 24 h

incubation, the treated cells were washed three times with fresh cell medium to remove any unbound nanoparticles. A 100 μL aliquot of an MTT solution (2.5 mg/mL in PBS) was added to each treated well and control. The cells were incubated for 4 h at 37 °C; then, the cell medium was removed, and a 100 μL aliquot of dimethylsulfoxide (DMSO) was added, in order to solubilize water-insoluble formazan that is formed by reduction of MTT agent by live cell enzymes. The cell viability is determined by measuring light absorbance of each well at a wavelength of 550 nm and comparing the results with those of controls.

RESULTS AND DISCUSSION

Dye Loading and Sensitivity. We optimized two important sensing characteristics, (1) oxygen sensitivity and (2) brightness (luminescence intensity), through control of the interaction between the PAA matrix and the G2 dye. Note that for in vitro and in vivo optical sensing, where one encounters many interfering luminescence signals, high dye loading per nanoparticle is very advantageous, as it enhances the luminescence intensity of the sensor. The sensitivity of a nanoparticle sensor usually depends on that of the incorporated indicator dye. However, it has been reported that matrix composition could affect the sensitivity. For example, ormosil serves better than silica as a matrix for oxygen sensing, as the presence of organic side groups increases the matrix oxygen solubility as well as its permeability.[25,41,42] We hypothesized that, for a given matrix and an indicator dye, the interaction between the matrix and the dye would affect both the dye loading efficiency and the matrix permeability toward analytes, affecting the brightness and sensitivity of the sensors, respectively. Note that the G2 dye is highly negatively charged, with 16 carboxyl groups,[13] which can be utilized for enhanced charge−charge interaction between G2 and the positively charged amine-functionalized PAA (AFPAA) or for covalent linkage to G2 (Figure 1a). The nanoparticle matrix composition, the G2 loading methods, and the G2 input amount were varied, so as to optimize the dye loading and sensitivity of the nanosensors, as summarized in Table 1.

The results from the G2-encapsulated nanosensors (Enc-PAA and Enc-AFP in Table 1) show that the dye loading efficiency increased drastically (about 30 times) but the sensitivity decreased significantly (about 2 times based on R_{N2}/R_{O2}, an intensity ratio under nitrogen and oxygen), by switching the matrix from PAA to AFPAA. The charge−charge interaction seems to help boost the dye loading efficiency but reduce the oxygen sensitivity by formation of more densely packed structures around G2 within the nanoparticle. We have incorporated an excess molar amount of APMA, with respect to G2, within the nanoparticles so as to have enough amine groups available for the TAT or F3 peptides. When the APMA/G2 molar ratio, a key factor for the charge−charge interaction, was increased from 188 to 540, the G2 loading efficiency stayed almost constant but its oxygen sensitivity decreased (R_{N2}/R_{O2} from 17 to 9.9). In contrast to the above, the results from G2-covalently linked nanosensors (Cov-AFP) show that covalent bonding can enhance both the dye loading efficiency and the sensitivity.

(39) Beckmann, J. S.; Wink, D. A.; Crow, J. P. In *Methods in Nitric Oxide Research*; Feelisch, M., Stamler, J. S., Eds.; John Wiley & Sons: New York, 1996; pp 61−70.

(40) Lide, D. R. *Handbook of Chemistry and Physics*, 82nd ed.; CRC Press: Boca Raton, 2001.

(41) Ciriminna, R.; Pagliaro, M. *Analyst* **2009**, *134*, 1531–1535.

(42) Chu, C.; Lo, Y. *Sens. Actuators, B* **2009**, *124*, 376–382.
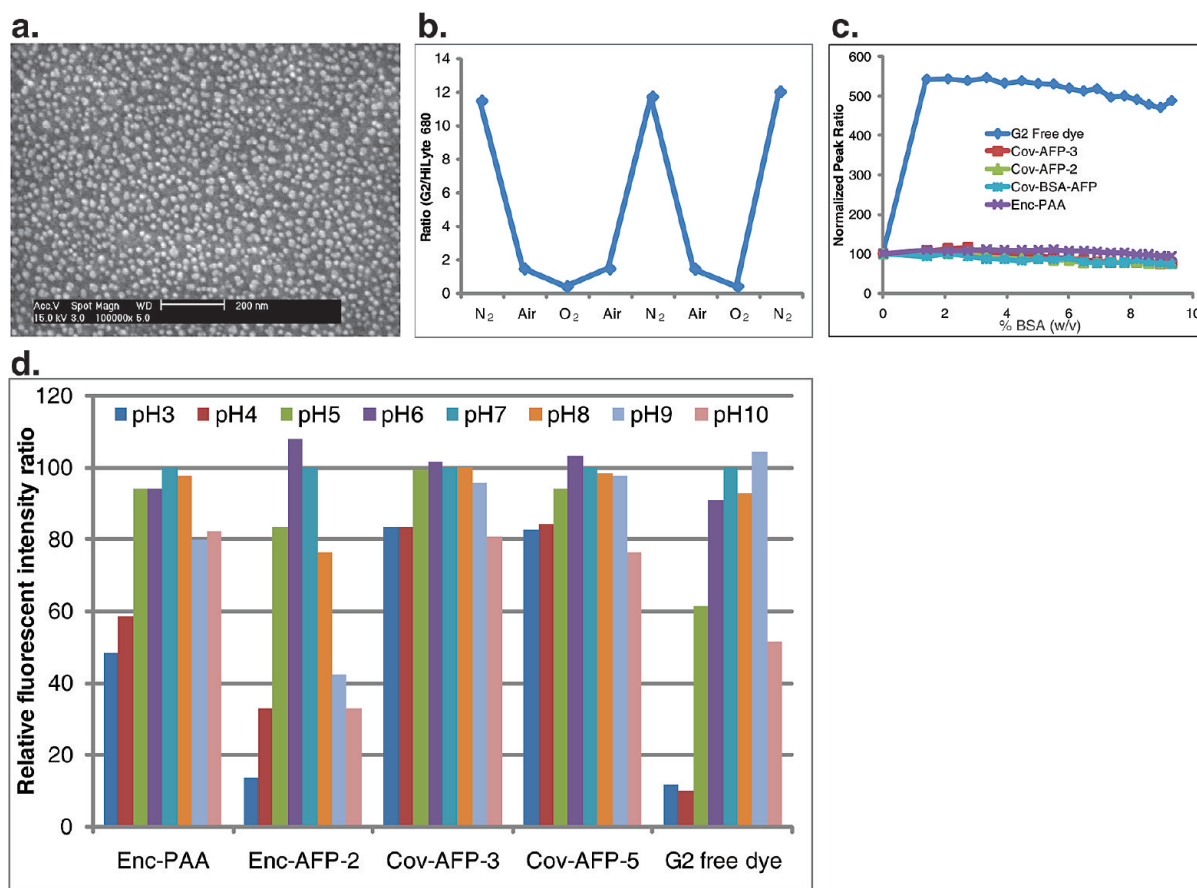
Figure 2. Oxygen nanosensor characterization. (a) A SEM image of Cov-AFP-3; (b) reversibility of Cov-AFP-3 measurements; (c) BSA interference (0−9.3% w/v); (d) pH interference (pH 3−10). The luminescence intensity ratios of G2/reference dye at pH 7 for each nanosensor are set to be 100. In the case of G2 free dye, the reference dye was included in the solution for the BSA and pH interference tests. The nanosensors showed a reversible response to oxygen levels and greatly improved stability in the presence of NO, BSA, and pH change in comparison with free oxygen probe G2.

The dye loading efficiency of Cov-AFP increased up to 100 times that of Enc-PAA, which is 3 times higher than that of Enc-AFP. The luminescence intensity, i.e., brightness, of Cov-AFP-3, -4, and -5 (see Table 1) was found to be proportional to the G2 loading. Note that each Cov-AFP-5 has about 700 times more G2 molecules than each Enc-PAA. Indeed, Cov-AFP-3, -4, and -5 showed the highest sensitivity among all G2-PAA nanosensor preparations, close to the highest previously reported sensitivity of hydrophobic oxygen nanosensors,[25,29] despite the use of a hydrophilic matrix. This may be partly attributed to the nanosensors' size, 4−8 times smaller than the previous nanosensors, that may reduce, by the same factor, the oxygen diffusion distance before meeting the probes within matrix.[20] However, the covalent bonding should still have played a major role for that because Cov-AFP-3 showed much higher sensitivity than Enc-AFP-2, despite the same molar ratio of APMA/G2. The covalent bonding was designed to prevent APMA molecules from crowding around each G2, alleviating the extent of the charge−charge interaction. The extent of covalent bonding between G2 and APMAs, the number of APMA molecules conjugated to a single G2 molecule, depends on the molar ratio of EDC/G2 as well as that of APMA/G2. The ratios of APMA/G2 and EDC/G2 for optimal dye loading efficiency and oxygen sensitivity are found to be below 188 and 18, respectively, under the current synthetic conditions. Such control of dye loading and sensitivity, based on the interaction

between dye molecules and nanoparticle matrix, was not possible for previously reported oxygen nanoparticle sensors in which dyes were just encapsulated in a nanoparticle matrix of fixed composition.[19] It should be also pointed out that, in a couple of previous ion sensor designs, strong interaction, i.e., covalent bonding, between dyes and nanoparticle matrix, was utilized to prevent dye leaching but not for changing the sensing characteristics.[43,44] Encapsulation of bovine serum albumin (BSA) within Cov-AFP was tried, with an expectation of enhancing the brightness, based on our observation of BSA interference (see Figure 2). However, both the loading efficiency and the oxygen sensitivity were reduced drastically, in comparison to Cov-AFP-3, its counterpart with no BSA. It appears that only a part of the BSA was encapsulated within the nanoparticles and that the binding between highly charged BSA and G2 reduces the oxygen permeability around G2, which consequently reduces the dye loading efficiency as well as the sensitivity.

Characterization. The nanosensors' size stayed uniform, around 30 nm in diameter when determined by SEM (see a typical image in Figure 2a), irrespective of dye loading methods, matrix compositions, and surface-conjugated peptides (see more SEM

(43) Almdal, K.; Sun, H.; Poulsen, A. K.; Arleth, L.; Jakobsen, I.; Gu, H.; Scharff-Poulsen, A. M. *Polym. Adv. Technol.* **2006**, *17*, 790–793.
(44) Hammond, V. J.; Aylott, J. W.; Greenway, G. M.; Watts, P.; Webster, A.; Wiles, C. *Analyst* **2008**, *133*, 71–75.

images in Figure S-1 in Supporting Information). The size distribution of the nanosensors in an aqueous solution was also determined by DLS. There is no significant difference in hydrodynamic size for different constructs of the nanosensors, either. However, the average hydrodynamic size was 51 ± 5 nm in diameter, which is a much larger value than the size determined by SEM, indicating that, as expected, the PAA nanoparticles are swollen in aqueous solutions. Please note that the nanosensors are smaller and more hydrophilic than previously reported oxygen nanosensors,[19] making them more favorable for biological applications. The surface charge of Enc-AFP and Cov-AFP are positive and almost the same (30 ± 6 mV) while that of Enc-PAA is slightly negative (−11 mV), as measured by a zeta-meter. The nanosensors are highly soluble in PBS (>100 mg/mL). There are no notable spectral shifts in the G2 absorption and luminescence peaks among the various preparations. Moreover, there was no detectable leaching, out of the nanoparticles in PBS, of the G2 dye, or of the reference dye, for all nanosensor preparations over a day. An extended dye leaching test for the Cov-AFP-5, under longer time and physiologically mimicking conditions, namely at 37 °C in 9% albumin containing PBS over a 3-day period, also showed no detectable dye leaching. The response, the intensity ratio of G2/reference, was reversible (Figure 2b). The upper limit of sensor's response time was about 0.4 s when measured as described previously.[29] There was greatly improved photostability over the "naked" (free) G2 dye; for instance, the half-life of Cov-AFP-5 was 39 min while that of free G2 was only 3 min, under continuous illumination by 630 nm light (1.5 mW) and under air-saturated conditions (see Figure S-2 in Supporting Information for photobleaching profiles of free G2 and nanosensor (G2 and reference dye)). Cov-AFP-3 showed no change in response after 1 h illumination at 135 μW: the typical power used in this study. Under nitrogen-saturated conditions (0% oxygen), no photobleaching, of either the G2 dye or the G2-loaded nanosensors, was observed. The amounts of TAT and F3 peptides per nanosensor were 0.015 and 0.027 μmol/mg NP, respectively.

Selectivity. A reliable biological sensor should be able to measure an analyte selectively, with minimal interferences from other chemical species that may occur in live cells and in vivo. Three potential interfering factors, pH, NO, and proteins, were tested, because of the following reasons: (1) The pH of cellular cytoplasms, and that of normal tissues and blood, is typically kept constant to be 7.2−7.4. However, the pH is significantly lower in some cellular domains (for example, the pH in the lysosome is only about 5) and can be changed due to various mechanisms.[45] Note that the nanoparticles that are endocytosed into cells may be directed into the lysosomes. Also, the pH inside tumor tissue has been reported to be slightly acidic.[46,47] (2) Regarding NO, it plays an important role in the maintenance of the cellular metabolism at hypoxia[48] and has been reported to affect the
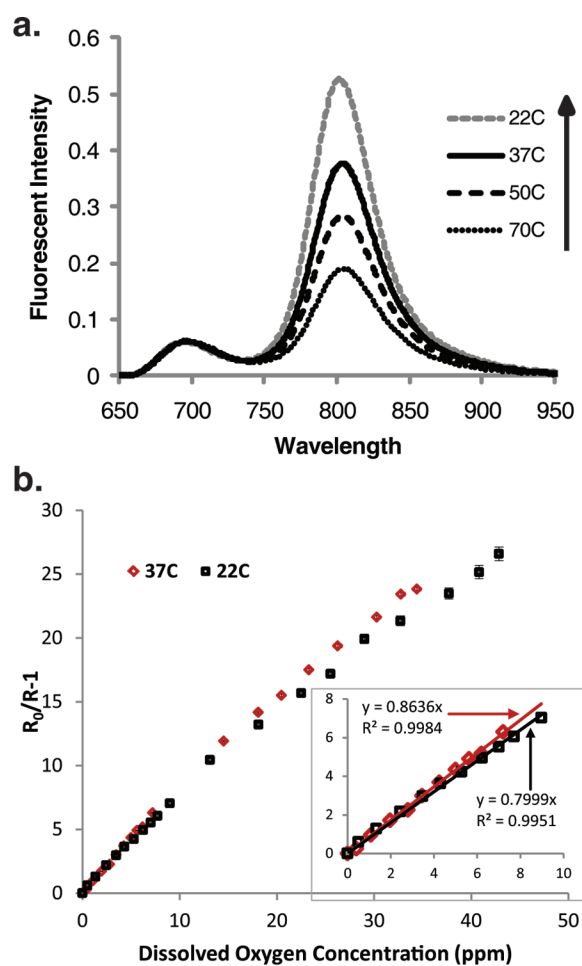

Figure 3. Temperature-dependent calibration curves. (a) Spectra of Cov-AFP-3 suspension in water at four different temperatures. The spectra were taken under a nitrogen-saturated environment; (b) Stern−Volmer calibration curves of Cov-AFP-3 at 22 and 37 °C. The Stern−Volmer plots were linear in the physiological range, 0% oxygen to air-saturated condition (see the inset plots). A representative series of the spectra used for the calibration curve is shown in Figure S-3 in Supporting Information.

response of other luminescence quenching-based oxyphores.[49] (3) Proteins often bind with molecular probes and change their response.[50] The test results show that the nanosensor's response is much less interfered by BSA, pH, or NO than that of the free indicator dye. While the presence of BSA (>0.3%) causes a substantial intensity increase (~550%) for the free G2 dye, it causes none for the nanosensors (Figure 2c).

An NO concentration of 150 ppb, much higher than the physiological concentration of NO (0.03−30 ppb),[51] causes negligible response change (<2%) for Cov-AFP but notable changes for Enc-PAA, Enc-AFP, and free G2, namely 11%, 18%, and 32%, respectively. The pH interference was also different for different nanosensor preparations (Figure 2d), but the order of stability was the same: Cov-AFP > Enc-PAA > Enc-AFP. For instance, the response of Cov-AFP-3 shows less than 1% variation between pH 5 and 8. Such drastically reduced interferences may be attributed

(45) Lee, E. S.; Gao, Z.; Bae, Y. H. *J. Controlled Release* **2008**, *132*, 164–170.
(46) van Sluis, R.; Bhujwalla, Z. M.; Raghunand, N.; Ballesteros, P.; Alvarez, J.; Cerdan, S.; Galons, J. P.; Gillies, R. J. *Magn. Reson. Med.* **1999**, *41*, 743–750.
(47) Ojugo, A. S. E.; McSheehy, P. M. J.; McIntyre, D. J. O.; McCoy, C.; Stubbs, M.; Leach, M. O.; Judson, I. R.; Griffiths, J. R. *NMR Biomed.* **1999**, *12*, 495–504.
(48) Palacios-Callender, M.; Quintero, M.; Hollis, V. S.; Springett, R. J.; Moncada, S. *Proc. Natl. Acad. Sci. U.S.A.* **2004**, *101*, 7630–7635.

(49) Papkovsky, D. B.; Desyaterik, I. V.; Ponomarev, G. V.; Kurochkin, I. N.; Korpela, T. *Anal. Chim. Acta* **1995**, *310*, 233–239.
(50) Park, E. J.; Brasuel, M.; Behrend, C.; Philbert, M. A.; Kopelman, R. *Anal. Chem.* **2003**, *75*, 3784–3791.
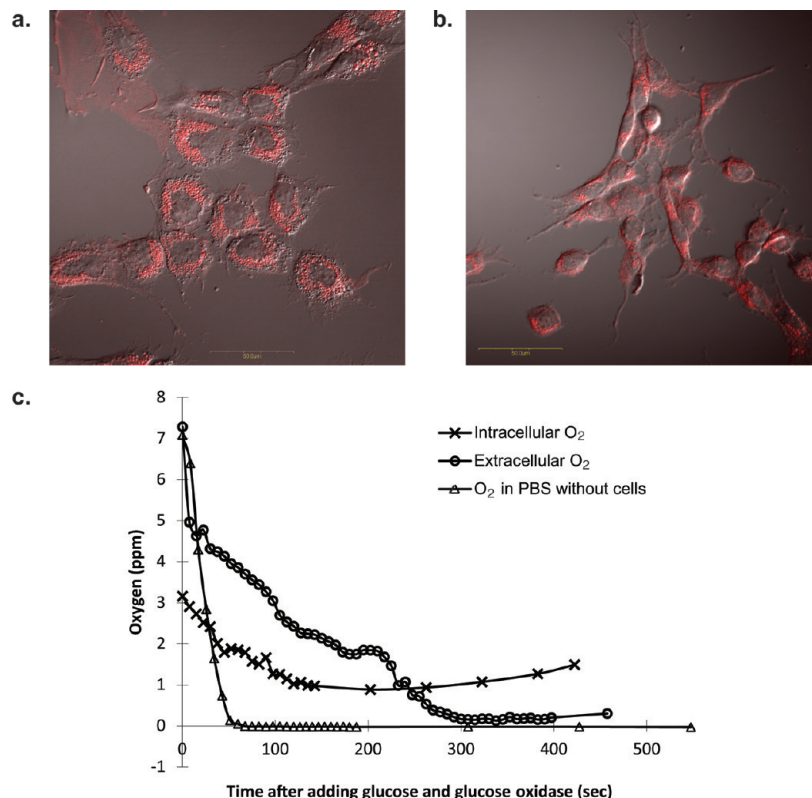(51) Brown, G. C. *FEBS Lett.* **1995**, *369*, 136–139.

Figure 4. Intracellular oxygen measurements. (a) Confocal images of live C6 glioma cells loaded with Cov-AFP-3 nanosensors by endocytosis after overnight incubation (20 h) with 100× magnification. (b) Those by TAT-peptide assisted delivery after 2 h incubation with 60× magnification. The confocal images were obtained by the fluorescence of Hilyte 680 dye molecules, used as reference fluorophores in the nanosensors. (c) Response of endocytosed nanosensors within and outside A549 cells as well as in PBS after D-glucose and glucose oxidase are added. The experimental conditions for measuring O_2 in PBS without cells were exactly the same as for the intra- and extracellular O_2 except for the presence of the cells. The response was monitored by taking the spectra of the nanosensors at 40× magnification. The intracellular oxygen concentration is lower than the extracellular concentration. Both intra- and extracellular oxygen concentrations change slowly compared to oxygen concentration in PBS after the addition of D-glucose and glucose oxidase.

to the modification of the G2 structure by the covalent bonding (especially regarding pH) and/or the nanoparticle's matrix, which efficiently blocks large (protein) or short-lived (NO) molecules.

Temperature Dependence and Calibration Curve. The oxygen sensing based on the luminescence-quenching mechanism has been reported to be temperature dependent.[52−54] The temperature dependence of the nanosensors was studied by taking the spectra under a nitrogen-saturated environment, at four different temperatures (Figure 3a). The oxygen-sensitive G2 intensity changed drastically with temperature, while the reference dye intensity remained the same. In consideration of the temperature-dependent response, a calibration curve at the working temperature (Figure 3b) was prepared from the spectra at different dissolved oxygen concentrations at the selected temperature (Figure S-3 in Supporting Information). The Stern−Volmer calibration plots, at 22 and 37 °C (Figure 3b), are slightly off from linear lines over the whole range of dissolved oxygen concentrations but are straight lines over the physiological range (0% oxygen up to air-saturated level). The slope and, hence, the sensitivity are higher at 37 °C than at 22 °C, presumably due to the increased oxygen diffusion rate within the nanoparticle matrix at the higher temperature. The calibration curve at 37 °C was utilized for the

intracellular measurements reported below. Note that, often before, intracellular measurements with nanosensors were based on calibration curves taken at ambient temperature, without considering the temperature dependence.

Intracellular Oxygen Measurements. The Cov-AFP-3 nanosensors were applied for measurements in two cell lines, C6 glioma and A549 human lung adenocarcinoma. The intracellular delivery of the nanosensors was diversified, with three different methods: endocytosis, TAT peptide assisted delivery,[55] and gene-gun delivery.[25] The TAT-linked nanosensors were internalized by the cells much faster than the unmodified nanosensors, requiring at least 4 times shorter incubation times to obtain the same intensity level. This indicates a successful conjugation of the TAT peptide to the nanoparticle surface, as well as the existence of different mechanisms for TAT peptide assisted delivery and endocytosis. The fluorescent confocal images of the cells, with nanosensors delivered by endocytosis or TAT peptide, indicate that the nanosensors are localized inside the cells but not in the nuclei (Figure 4a,b). The gene-gun delivered nanosensors were also localized in the cytoplasm (data not shown), as in previous studies.[25] Internalization of the nanosensors within cells was confirmed by taking z-series images. It is noticeable in Figure 4a that the cells continue to divide after incubation with nanosensors (4 mg/mL) for 20 h. This demonstrates that the nanosensors are

(52) Coyle, L. M.; Gouterman, M. *Sens. Actuators, B* **1999**, *61*, 92–99.
(53) Mongey, K. F.; Vos, J. G.; MacCraith, B. D.; McDonagh, C. M.; Coates, C.; McGarvey, J. J. *J. Mater. Chem.* **1997**, *7*, 1473–1479.
(54) Borisov, S. M.; Wolfbeis, O. S. *Anal. Chem.* **2006**, *78*, 5094–5010.

(55) Webster, A.; Compton, S. J.; Aylott, J. W. *Analyst* **2005**, *130*, 163–170.
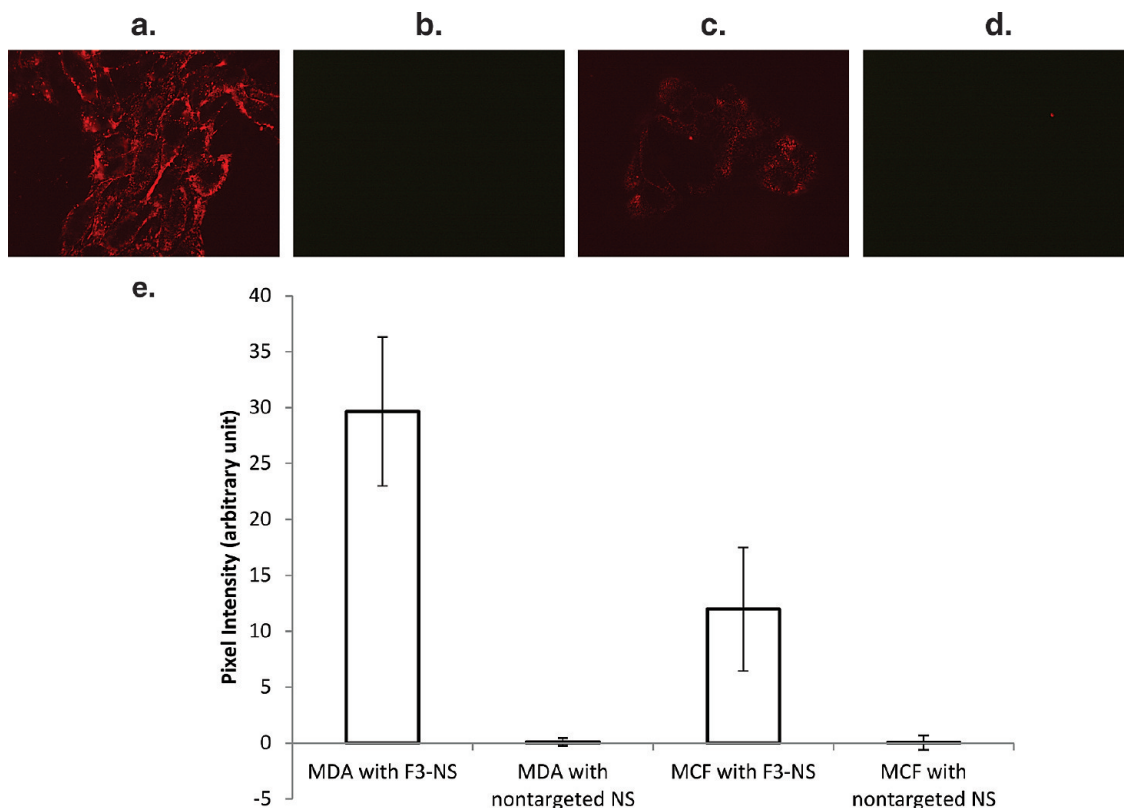
Figure 5. Target-specific delivery of F3-linked nanosensors (a−d). Confocal images of MDA-MB-435 cells treated with F3-targeted nanosensors (F3-NS; a) and nontargeted ones (b), and the images of MCF-7 cells with F3-NS (c) and nontargeted ones (d). (e) Relative cell binding of F3-targeted and nontargeted nanosensors, estimated by pixel intensity of the luminescent images. The surface-conjugated F3 peptides enable the nanosensors to target specific cells selectively.

nontoxic and noninvasive. Note that the cell growth (or reproduction through division) is a strong indication for healthy cell conditions. The MTT assay results also confirmed that the nanosensors do not affect cell viability and, therefore, are nontoxic (Figure S-4 in Supporting Information).

The intracellular oxygen concentrations were measured by taking the spectra of nanosensors internalized within cells. The intracellular nanosensors' spectra were free from cellular autofluorescence (Figure S-5 in Supporting Information). The average intracellular oxygen concentrations under normal conditions, i.e., cells with a cell medium exposed to air, were determined from the average values at 10−20 different spots. At each spot, a circular area on a cell-containing cover glass where the light is illuminated and having a size of ∼520 μm in diameter at 40× magnification, measurements were performed 3 to 4 times consecutively, with a delay of 1 to 2 s after each measurement that took 100 ms. There was no notable difference in the measured concentrations with different delivery methods. The average intracellular oxygen concentrations were 4.9 ± 1.2 ppm (110 ± 27 mmHg) in the C6 glioma cells and 4.5 ± 1.0 ppm (99 ± 22 mmHg) in the A549 cells. It should be noted that the measured oxygen concentrations are not significantly affected by the presence of nanosensors and illumination under our experimental conditions, because of the following reasons: (1) The difference between individual measured values was negligible. (2) The upper limit of moles of consumed oxygen molecules during a measurement, is calculated, on the basis of the intracellular concentrations of the nanosensors, as

well as under the extreme assumption[56] that each triplet excited state G2 molecule converts a ground state oxygen molecule into a singlet oxygen molecule, giving 10 nM (0.3 ppb). This is 3 to 4 orders of magnitude below the uncertainty of ∼1 ppm reported in the measured oxygen concentrations. The amount of nanosensors per cell was estimated to be 1.4×10^{-7} mg per cell from the absorbance measurements of the cells containing nanosensors and each cell was assumed to be a sphere of about 15 μm in diameter. It should be also noted that the phototoxicity of the nanosensors was tested by measuring singlet oxygen produced from the nanosensors using a chemical probe, as well as by cell kill using a live/dead cell assay as described in our previously published paper.[57] Under the same experimental conditions, the nanosensors neither produced detectable singlet oxygen nor killed the cells and, therefore, are not phototoxic. However, the nanosensors produced singlet oxygen and killed the cells when we applied the light for more than 6 min, about 1000 times longer than the period we used for sensing. This suggests that prolonged exposure to the light should be avoided to avoid phototoxicity problems.

The intracellular oxygen concentrations were monitored under a hypoxic extracellular condition that was induced by adding D-glucose and glucose oxidase to the cell medium (10 mM and 10 units per mL, respectively). The extracellular oxygen concen-

(56) Vanderkooi, J. M.; Maniara, G.; Green, T. J.; Wilson, D. F. *J. Biol. Chem.* **1987**, *262*, 5476–5482.
(57) Tang, W.; Xu, H.; Kopelman, R.; Philbert, M. A. *Photochem. Photobiol.* **2005**, *81*, 242–249.

tration and the oxygen concentration in PBS without cells were also monitored, immediately after adding the nanosensors to the samples, under the same induced hypoxic condition for comparison. As shown in Figure 4c, the nanosensors were able to monitor the changes in oxygen concentrations under the induced hypoxic condition. Interestingly, these intracellular measurements result in the following important findings. First, intracellular oxygen concentrations are considerably lower (only ~65%) than the oxygen concentration of air-saturated water at 37 °C, i.e., 7.2 ppm. Second, the presence of the cells subdues the changes of oxygen concentration not only inside but also outside the cells. The intracellular oxygen concentration, already initially lower than the extracellular concentration or air-saturated PBS, showed the least changes. We performed the same test with TAT-linked nanosensors (data not shown), observing the same trend: smaller and slower changes inside cells than outside cells. Third, there is a slight difference (~8%) between the measured intracellular oxygen concentrations in two different cell lines. It has been reported that every cell type is able to sense hypoxia and to react through several pathways, which may differ in different cell types, in order to maintain oxygen homeostasis.[58] The cells' responses against hypoxia can be estimated by the posthypoxia expression levels of hypoxia-inducible factors.[59] It should be noted that our nanosensors were able to show, in real time, the existence of cellular activities aimed at maintaining the oxygen homeostasis, within a single cell, according to the first and second observations. The third observation suggests that the intracellular oxygen level may be regulated differently in different cell types, as also noted by others.[60,61] This may require further investigation, with more precisely controlled cellular parameters, such as cell density.

Targeting of Nanosensors to Specific Cancer Cells. For enhanced selective tumor targeting, nanosensors conjugated with F3 peptides were prepared and tested in vitro. The F3 peptide is known to bind to the angiogenic vasculature within solid tumors, as well as to some tumor cells, by interacting with nucleolin, a cell surface receptor.[62] Two cancer cells, high nucleolin-expressing MDA-MB-435 and low nucleolin-expressing MCF-7, were treated with F3-conjugated nanosensors. As shown in Figure 5, the F3-linked nanosensors bound to both cell lines but with about 2.5 times higher binding efficiency to MDA-MB-435 cells than to MCF-cells, demonstrating their selectivity to specific target cells. The binding of nontargeted nanosensors to both cell lines was negligible, indicating that nonspecific binding of the nanosensors to the cells is insignificant.

CONCLUSIONS

In summary, targeted ratiometric nanosensors have been developed to enable noninvasive quantitative measurements of oxygen in live cells. The sensors are made of PAA hydrogel nanoparticles loaded with oxygen-sensitive dyes and oxygen-insensitive dyes, both emitting NIR luminescence that is free from cellular autofluorescence as well as from light absorption and scattering in live tissue, and with an addition of surface-conjugated peptides. These sensors were engineered for high sensitivity and brightness by manipulating the interactions between the nanoparticle matrix and the oxygen-sensitive dye through variations in the G2 loading methods, G2 amount, and nanoparticle matrix composition. The sensors' response is linear over the physiological oxygen range and does not change in the presence of 150 ppb NO or 9% protein (BSA) as well as a pH variation between 5 and 9. The sensors were used successfully for reliable real-time oxygen measurements and time monitoring, inside live tumor cells under normal and hypoxic conditions. The noninvasiveness and non-toxicity of the nanosensors were demonstrated by the continuous division of the cells during the 20 h long presence of high amounts of these sensors as well as MTT assay results. The phototoxicity of the nanosensors was also negligible under the experimental conditions used. These nanosensors are expected to be applicable for tumor hypoxia measurements with potentially high in vivo selectivity for tumors, enabled due to their proper size, their high aqueous solubility, and their surface-labeled tumor-specific targeting moieties.

SUPPORTING INFORMATION AVAILABLE

Additional information as noted in text. This material is available free of charge via the Internet at http://pubs.acs.org.

(58) Wenger, R. H. *J. Exp. Biol.* **2000**, *103*, 1253–1263.
(59) Semenza, G. L. *Cell* **2008**, *133*, 206–208.
(60) Ji, J.; Rosenzweig, N.; Jones, I.; Rosenzweig, Z. *Anal. Chem.* **2001**, *73*, 3521–3527.
(61) O'Riordan, T. C.; Fitzgerald, K.; Ponomarev, G. V.; Mackrill, J.; Hynes, J.; Taylor, C.; Papkovsky, D. B. *Am. J. Physiol. Regul. Integr. Comp. Physiol.* **2007**, *292*, R1613–R1620.
(62) Christian, S.; Pilch, J.; Akerman, M. E.; Porkka, K.; Laakkonen, P.; Ruoslahti, E. *J. Cell Biol.* **2003**, *163*, 871–878.